Journal of Applied Fluid Mechanics, Vol. 12, No. 6, pp. 2031-2038, 2019.
Available online at www.jafmonline.net, ISSN 1735-3572, EISSN 1735-3645.
DOI: 10.29252/jafm.12.06.29789

Numerically Determined Empirical Relationships for a Transitional Turbulence Model

G. Erfort†, T. W. von Backström and G. Venter

Mechanical and Mechatronic Engineering, Stellenbosch University, Stellenbosch, 7800, South Africa

† *Corresponding Author Email: erfort@sun.ac.za*

(Received October 26, 2018; accepted March2, 2019)

ABSTRACT

Turbulence models in computational fluid dynamics (CFD) aim to capture a complex phenomenon through simplified mathematical models. The models themselves range in terms of application, complexity and methodology. This work looked at a transitional model for Reynolds averaged Navier Stokes equations. In particular the focus was on the correlation based intermittency and momentum thickness Reynolds number (γ - $\tilde{Re}_{\theta t}$) model. The original model has high order correlations, that were determined and calibrated from flat plate tests of various pressure gradients. In this work the correlations were simplified to reduce the number of calibration coefficients and help in understanding the effect of each parameter. Flat plate test data, from the European Research Community on Flow, Turbulence and Combustion (ERCOFTAC) T3A series, were used to verify the lower order approximations through OpenFOAM simulations. The open source CFD package OpenFOAM was used for its easy access to the base code. The reduced order model was then applied to a National Advisory Committee for Aeronautics (NACA) 0012 foil at a transitional Reynolds number of 360 000 as a means of validation. The reduced order, the original γ - $\tilde{Re}_{\theta t}$ and the fully turbulent k - omega shear stress transport (k − ω SST) turbulence models are compared over a range of angles of attack to highlight the difference between models. The proposed model reduced the runtime of simulation by approximately 6%. The reduction in model coefficients meant a step by step adjustment could be implemented to increase model accuracy. In addition the adjusted model increased the accuracy of drag prediction on a NACA0012 airfoil, while maintaining a similar lift prediction as the original.

Keywords: Transitional turbulence model; Optimization; NACA foil; OpenFOAM; Flat plate.

NOMENCLATURE

C_l	lift coefficient
Cd	drag coefficient
C_f	skin friction coefficient
E_*	destruction term
dU/ds	acceleration along a streamline
F_{length}	transition zone length
k	turbulent kinetic energy
P_*	production term
r	pearson correlation coefficient
Re	Reynolds number
$\tilde{Re}_{\theta t}$	local transition onset momentum thickness Reynolds number
Re_c	critical momentum thickness Reynolds number
$Re_{\theta t}$	transition onset momentum thickness Reynolds number
Tu	turbulence intensity
U	velocity
ν	kinematic viscosity
x/C	non-dimensional location along airfoil
y^+	non-dimensional wall distance
γ	intermittentcy
μ	dynamic viscosity
μ_t	turbulent dynamic viscosity
ω	specific dissipation
ρ	density
λ_θ	pressure gradient
θ	momentum thickness
σ_*	model constants
α	angle of attack

1. INTRODUCTION

Transition from laminar to turbulent flow is a complicated phenomenon that is closely linked to aero-dynamic stall. The factors affecting this phenomenon include geometry and free stream

turbulence intensity. Computationally expensive methods like Large Eddy Simulations or Detached Eddy Simulations are able to predict turbulence with greater accuracy than more commonly used Reynolds Averaged Navier Stokes (RANS) equations. The most common turbulence models in RANS simulations are fully turbulent. There are however transitional models, that attempt to describe the transition process of laminar to turbulent flow.

Transitional transport models are not new in the field of CFD, having being reported as early as the 1990s. Vicedo *et al*. (2004) proposed one such transport model that was applied in the modelling of separation bubbles. At the time of publication the trend was to have mathematical models that were specific to certain geometries and flow parameters, thus limiting their applicability. The authors developed a model that required no normal-to-wall distance and related transition onset to the local momentum thickness Reynolds number. Langtry and Menter (2005) authored a paper outlining a correlation based transition model which was based entirely on local variables, namely a transition momentum thickness Reynolds number ($\tilde{R}e_{\theta t}$) and intermittency (γ). The model uses two additional transport equations, for intermittency and transition onset criteria. Since the model is based entirely on local variables, it is compatible with unstructured meshes and well suited for parallelization. The model does not try to describe the physical process but instead is based on empirically determined relationships. Upon publication, Langtry and Menter did not release their original correlations but subsequent authors using their framework have presented their findings while using the transition model. Toyoda *et al*. (2007) made use of the correlation approach to predict boundary layer transition on the JAXA high-lift configuration model. The authors applied their own empirical correlations to compare the lift and drag results as well as the skin friction for identifying the start of intermittency. Their results indicated that the model was not able to handle a large cross flow velocity. Sorensen (2009) attempted to determine the empirical relationships for the correlation model and verified the results with tests on two different aerofoils and a wind turbine rotor.

The correlations supplied by Toyoda *et al*. (2007) and Sorensen (2009) were not in agreement indicating the possibility of correlations being specific to geometry and flow conditions.

Langtry and Menter (2009) released their empirical relationships for the length of the transition region (F_{length}), critical Reynolds number ($Re_{\theta c}$) indicating where transition first increases within the bound-ary layer, and transition onset Reynolds ($Re_{\theta t}$), which is a function of pressure gradient and turbulence intensity. Comparing the empirical relationships from Toyoda *et al*. (2007), Sorensen (2009) and Langtry and Menter (2009), a reasonable assumption could be made on the expected relationship between each empirical relationship. Simple functions are proposed for each empirical relationship and verified against flat plate test data, from the ERCOFTAC T3A (Savill, 1993; Savill 1996) series. The NACA 0012 airfoil was then simulated at transitional Reynolds numbers and validated against experimental data from Sheldahl and Klimas (1981). For all the simulations the transition model is compared against the fully turbulent $k\omega$ model to highlight their differences in turbulent kinetic energy.

2. THE $\gamma - \tilde{R}e_{\theta t}$ MODEL

The $\gamma - \tilde{R}e_{\theta t}$ model is a four-equation model that couples to the k −ω SST model. The two additional transport equations are for intermittency (γ) and transition momentum thickness Reynolds number ($\tilde{R}e_{\theta t}$). The equation for intermittency is

$$\frac{\partial(\rho\gamma)}{\partial t}+\frac{\partial \rho U_j \gamma}{\partial x_j}=P_\gamma-E_\gamma+\frac{\partial}{\partial x_j}\left[\left(\mu+\frac{\mu_t}{\sigma_f}\right)\frac{\partial \gamma}{\partial x_j}\right] \tag{1}$$

where the transition source is $P\gamma$ and the destruction source is $E\gamma$. The transport equation for transition momentum thickness Reynolds number is

$$\frac{\partial\left(\rho\tilde{R}e_{\theta_t}\right)}{\partial t}+\frac{\partial \rho U_j \tilde{R}e_{\theta_t}}{\partial x_j}= P_{\theta_t}+\frac{\partial}{\partial x_j}[\sigma_{\theta_t}(\mu+\mu_t)\frac{\partial \tilde{R}e_{\theta_t}}{\partial x_j}] \tag{2}$$

The source term $P_{\theta t}$ is used to ensure the trans-port variable $\tilde{R}e_{\theta t}$ matches the locally determined $Re_{\theta t}$ and γ is used as a trigger for transition while $\tilde{R}e_{\theta t}$ takes into account the non local effects of turbulence intensity. These non local effects include the decay of turbulence kinetic energy in the free stream and changes in velocity outside of the boundary layer. This equation is important as it brings together the empirical relationships which are used in the γ equation. Intermittency interacts with the traditional k − ω model through the destruction ($\tilde{D}_k$ = $min(max(\gamma_{eff},0.1)1.0)\, D_k$) and production terms ($\tilde{p}_k$ = $\gamma_{eff}\, P_k$) for turbulent kinetic energy. Full details of the model are provided in Langtry and Menter (2009).

Equations 3 to 6 are the piecewise empirical relationships as originally defined

$$\mathrm{Re}_{\theta_c} = \begin{cases} \tilde{R}e_{\theta_t} - (396.035\cdot10^{-2} - 120.656\cdot10^{-4}\tilde{R}e_{\theta_t} \\ +868.23\cdot10^{-6}\tilde{R}e_{\theta_t}^2 - 696.506\cdot10^{-9}\tilde{R}e_{\theta_t}^3 \\ +174.105.10^{-12}\tilde{R}e_{\theta_t}^4) & \tilde{R}e_{\theta_t} \le 1870 \\ \tilde{R}e_{\theta_t} - 593.11 + (\tilde{R}e_{\theta_t} - 1870)\cdot 0.482 & \tilde{R}e_{\theta_t} > 1870 \end{cases} \tag{3}$$

$$\begin{cases} 398.189\cdot10^{-1} - 119.27\cdot10^{-4}\tilde{R}e_{\theta_t} \\ -135.567\cdot10^{-6}\tilde{R}e_{\theta_t}^2 & \tilde{R}e_{\theta_t} \le 400 \\ 263.404 - 123.939\cdot10^{-2}\tilde{R}e_{\theta_t} + \\ 194.548\cdot10^{-5}\tilde{R}e_{\theta_t}^2 - \\ 101.695.10^{-8}\tilde{R}e_{\theta_t}^3 & 400 \le 596 \\ 0.5 - (\tilde{R}e_{\theta_t} - 596)\cdot 3\cdot10^{-4} & 596 \le 1200 \\ 0.3188 & 1200 \le \tilde{R}e_{\theta_t} \end{cases} \tag{4}$$

$$\tilde{Re}_{\theta_t} = \begin{cases} \left[1173.51 - 589.428Tu + \dfrac{0.2196}{Tu^2}\right] F(\lambda_\theta) & Tu \le 1.3 \\ 331.5\left[Tu - 0.5658\right]^{-0.671} F(\lambda_\theta) & Tu > 1.3 \end{cases} \quad (5)$$

$$F(\lambda_\theta) = \begin{cases} 1 - \left[-12.986\lambda_\theta - 123.66\lambda_\theta^2 - 405.689\lambda_\theta^3\right] \\ \exp\left(-\left[\dfrac{Tu}{1.5}\right]^{1.5}\right) & \lambda_\theta \le 0 \\ 1 + 0.275\left[1 - \exp(-35\lambda_\theta)\right]\exp\left(\dfrac{-Tu}{0.5}\right) & \lambda_\theta > 0 \end{cases} \quad (6)$$

Equations 5 and 6 are functions of turbulence intensity (T_u) and the pressure gradient coefficient

$$\lambda_\theta = \left(\frac{\theta^2}{\nu}\right)\frac{dU}{ds} \quad (7)$$

These correlations are not the only published models, however they are the original formulation and served as a starting point for approximating the relationships. Without investigating the physical process underlying the phenomena it would be impossible to discern a relationship between the $\tilde{Re}_{\theta t}$ and the empirical variables. Using the work of previous authors, shown in figure 1, we can infer the type of relationship for these variables. For example the $Re_{\theta c}$ straight line of Misaka and Obayashi (2006), the blended function of Sorensen (2009) and the high order function of Langtry and Menter (2009) match closely in the lower region, while the constant value assumed by Sorensen (2009) matches the assumption of Lanzafame *et al.* (2014) who prescribed a fixed value for the critical Reynolds number.

1. REDUCED ORDER MODEL

The complex equations defining the correlation functions do not lend themselves to easy interpretation. For example, inspection of equation 4 does not inform on the shape of the curve or how adjustment of any single coefficient would affect the final curve. A simpler model is proposed that captures a similar relationship but with fewer coefficients.

$$F_{length} = \frac{h}{\sqrt{2\pi\sigma^2}} \cdot e^{\frac{-\tilde{Re}_{\theta_t}^2}{2\sigma^2}} + C_{Ln} \quad (8)$$

Equation 8 is a Gaussian function that produced a similar curve shape to equation 4. Figure 2 shows the curves of two published relationships for F_{length} ($\tilde{Re}_{\theta t}$) and the Gaussian function proposed in this work. Equation 8, with 3 coefficients was fit-ted with a least squares optimization to match the shape of equation 4, which has 11 coefficients. In equation 8, h is the scale factor for adjusting the length of transition at lower momentum thickness Reynolds numbers, σ adjusts the variance, which controls the gradient of the curve and finally C is the limit of transition length. Figure 3 shows the effect of

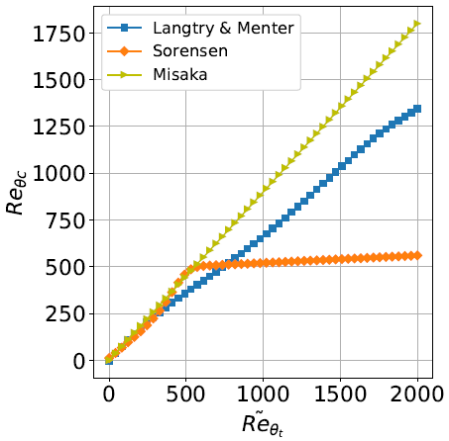

Fig. 1. $Re_{ec}(\tilde{Re}_{\theta t})$ as proposed by Langtry and Menter (2009), Sorensen (2009) and Misaka and Obayashi (2006).

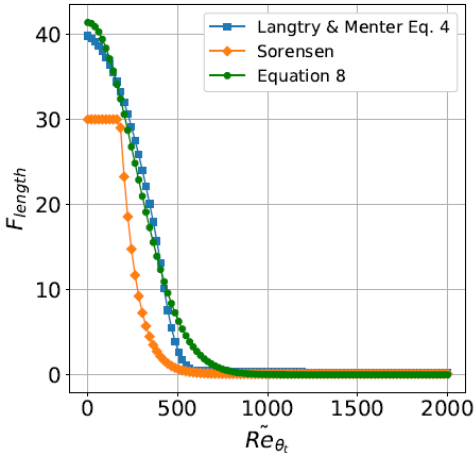

Fig. 2. $F_{length}(\tilde{Re}_{\theta t})$ as proposed by Langtry and Menter (2009) with 11 coefficients, Sorensen (2009) with 4 coefficients and the Gaussian function with 3 coefficients.

changing these individual parameters. The procedure of identifying a simple equation to replicate the piecewise curves, in the original formulation, resulted in equations 3 and 5 being approximated with The results of a least squares fit between previous works and equation 9 are shown in figure 4. In the lower $\tilde{Re}_{\theta t}$ region equation 9 follows the gradient of Langtry and Menter (2009) but switches to the constant value as per Sorensen (2009) at the intersection. The choice for a piecewise description for equation 9 allowed the solution to match any of 3 published relationships (Langtry and Menter, 2009; Sorensen, 2009; Lanzafame *et al.* 2014) without much effort.

$$Re_{\theta_c} = \begin{cases} m\tilde{Re}_{\theta_t} & \tilde{Re}_{\theta_t} \le \dfrac{c}{m} \\ C_c & \tilde{Re}_{\theta_t} \ge \dfrac{c}{m} \end{cases} \quad (9)$$

$$Re_{\theta_t} = (AB^{-Tu} + C_t) f(\lambda, TU) \quad (10)$$

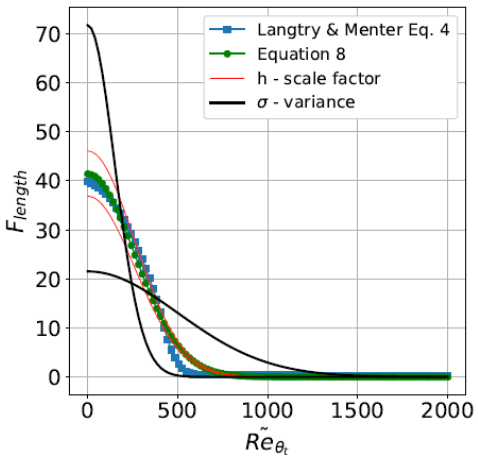

Fig. 3. Effect of altering parameters on the Gauss fit for F_{length}.

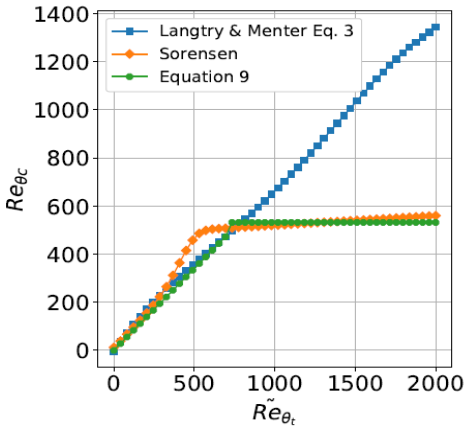

Fig. 4. Re_c as described by Equation 9, Langtry and Menter (2009) and Sorensen (2009).

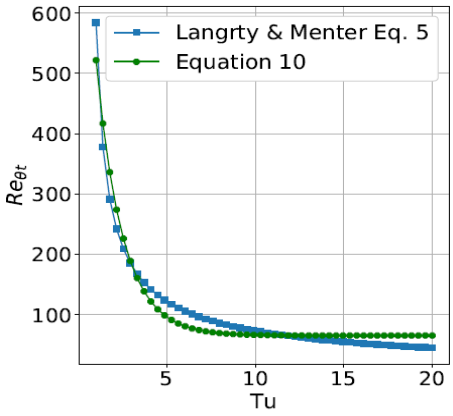

Fig. 5. The least squares best fit between $Re_{\theta t}$ as per Langtry and Menter (2009) and Equation 10.

Similarly figure 5 shows the fit between equation 10, which has only 3 coefficients, and equation 5 which has 6 coefficients.

2. NUMERICAL SIMULATION

To calibrate the new correlation coefficients a 2D model of the T3A test case from the ERFOTAC series was replicated in OpenFOAM (Weller *et al.* 1998). The flat plate test case was built with a hexahedral mesh consisting of 26820 cells. The domain was 3 m by 1 m in the X and Y axes respectively and with the boundary conditions as listed in Table 1.

Table 1 Flat plate boundary conditions

Patch	Type	BC
Inlet	velocity	fixed
Outlet	pressure	fixed
Top	slip	zero gradient
Plate	wall	fixed value

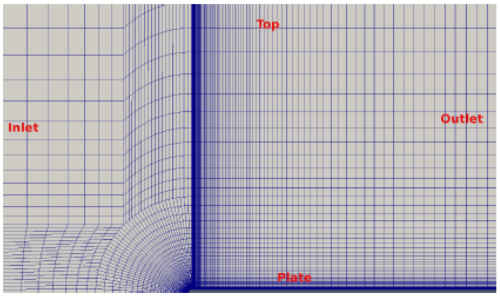

Fig. 6. T3A test case mesh, inlet and plate.

Figure 6 shows the refinement applied to the leading edge of plate and growth ratio used to minimize the number of cells required. The numerical simulation was constructed to replicate in as far as possible the set-up of the ERCOFTAC experiments (Savill, 1990).

For verification a 2D airfoil simulation was constructed on the NACA 0012 wing. The airfoil was set in the middle of a C mesh domain, 20 chord lengths away from each boundary patch. The domain size was based on work carried out by Vanderspuy (2011) where he performed 2D analysis on various airfoil profiles at a Reynolds number of 2 100 000. On this scale the foil is barely visible when looking at the full domain, as presented in figure 7. Table 2 provides the boundary conditions applied to each patch. The freestream patch in OpenFOAM switches between a fixed value and zero gradient condition depending on the sign of the flux.

The mesh was made up of 1.3 million cells with refinement on the airfoil surface to ensure a $y^+ \leq 1$. The simulation used the 2nd order self-filtered central differencing scheme. It was run in a steady state condition as the range of angles of attack (α) were all pre-stall. A Reynolds number of 360 000 was used in the simulations as it is within the transitional range for this foil.

Table 2 Flat plate boundary conditions

Patch	Type	BC
Inlet	velocity	freestream
Outlet	pressure	freestream
Top	pressure	freestream
Bottom	pressure	freestream
Airfoil	wall	fixed value

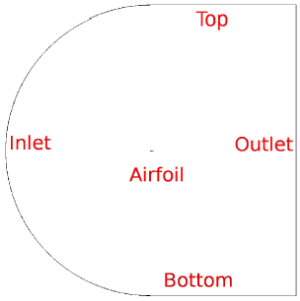

Fig. 7. C-MESH with boundary labels.

5. RESULTS

5.1 Best Fit Model

Equations 8, 9 and 10 were implemented into the turbulence model individually. The coefficients, resulting from the least squares best fit are presented in table 2 along with manually selected values, explained in section 5.2. The least squares fit minimizes the sum of squares of the offsets between two curves. The target curves are defined by equations 3 – 5 Figure 8 shows the skin friction coefficient (C_f) along the flat plate, for each individual substitution into the transition model as well as the results of a fully turbulent model. At higher Reynolds numbers the models converge to the experimental values. However at lower Reynolds numbers the fully turbulent model does not capture change in skin friction as a result of transitional behaviour. The F_{length} substitution had negligible effect, but the Rec equation caused earlier transition. $Re_{\theta t}$ resulted in the transition point being delayed, while all substitutions appear to have the same transition gradient.

Table 2 Coefficients for the simple mathematical models

Coefficient	Best fit value	Adjusted value
$F_{length} - h$	26941.88	28000
$F_{length} - \sigma$	259.89	180
$F_{length} - C_{Ln}$	0.02	-
$Re_c - m$	0.68	0.7
$Re_c - C_c$	532	-
$Re_{\theta_t} - A$	894.65	-
$Re_{\theta_t} - B$	1.96	3
$Re_{\theta_t} - C_t$	65.61	-

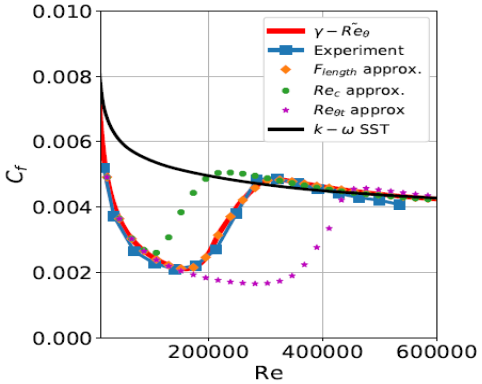

Fig. 8. C_f on T3A flat plate test case with single equation substitutions.

Figure 9 is the result of substituting all empirical relationships with the best fit values as per table 2.

Equations 9 and 10 had opposite effects on the transition point, however in combination the dominant relationship was $Re_{\theta t}$. The approximations proposed in this work were accurate over a range of Reynolds numbers, in representing the general shape of equations 3, 4 and 5. They were however not identical fits to the original, and their deficiency in capturing the original shape did not occur at the same Reynolds number. Thus in combination their cumulative build up in error resulted in an incorrect prediction for C_f . To compensate for this error build up adjustments had to be made to the coefficients of the new equations.

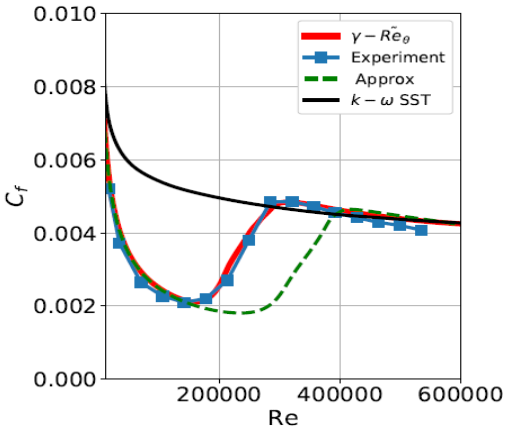

Fig. 9. C_f on T3A flat plate test case with all empirical relationships replaced by best fit solutions.

5.2 Adjusted Model

Equation 10 showed the most influence on C_f and was thus looked at first. The B value in the $Re_{\theta t}$ equation is responsible for the power relationship and allowed for the largest change with the smallest adjustment. Increasing the power meant $Re_{\theta t}$ was more sensitive to lower values of turbulence intensity. The change affected the transition gradient and caused earlier tripping. Equation 8 was then looked at to compensate for the transition gradient. Adjusting the scale and variance in the Gaussian function meant the transition length was extended at lower $Re_{\theta t}$. The root mean squared error (RMSE) between the experimental data and the reduced order model with these two adjustments was 7.5%. To delay tripping an increase in the Rec was made by adjusting the gradient of the straight line portion in equation 9. Increasing the gradient meant that the Reynolds number required to trigger transition was raised. The updated equations were then substituted into the model resulting in figure 10. By changing the coefficients in a methodical manner the error build up seen when combining each approximation has been compensated for.

Table 3 shows the Pearson correlation coefficient (r), as measure of linear correlation between the C_f predictions of the approximations and original model as well as the RMSE between the respective models

and experimental data. The table corroborates what is shown in figure 8, namely that substituting the F_{length} relationship in the transitional model has little effect on the reported C_f curve when compared to the original. However what is not clear in the image is that this single substitution outperforms the original model in terms of accuracy relative to the experimental data. With the adjusted coefficients the C_f curve again is acceptable in terms of shape with a Pearson correlation of 0.99 and performs less than 1% worse than the original model, when compared to experimental data.

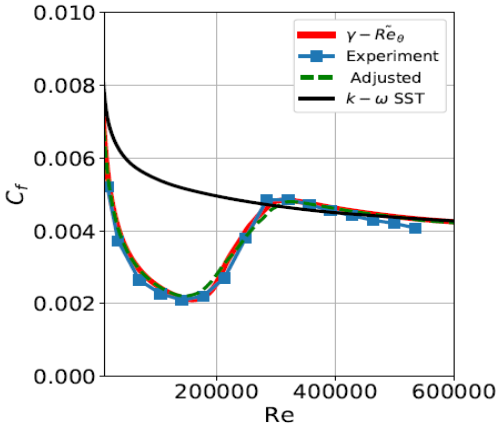

Fig. 10. C_f on T3A flat plate simulation with adjusted coefficients for the reduced order model.

Table 3 Curve metrics for flat plate tests

Model	r	RMSE as %
γ - $\tilde{Re}_{\theta_t}$	1	5.7
F_{length} sub	0.99	5.5
Reduced order	0.98	14.8
Reduced order adjusted	0.99	6.2

The fully turbulent k −ω SST , original γ - $\tilde{Re}_{\theta t}$ and reduced order model with adjusted coefficients were then run on a 2D NACA airfoil simulation. Using the (Sheldahl and Klimas, 1981) experimental data set the turbulence models were tested at the transitional Reynolds number of 360 000 through the linear range of the C_l vs α curve. Figure 11 shows the minimal variation in C_l between 1 and 10° angle of attack.

There is no difference in result between the reduced order model and the original formulation. However when looking at C_d , figure 12, the difference between models becomes more evident. The reduced order model actually outperforms or equals the drag prediction for the same range of α, by more closely matching the experimental results.

By examining the flow at 8° and looking at the wall shear stress we can identify the tripping point on the foil surface. Figure 13 shows the estimated wall shear stress based three turbulence models. The fully turbulent model never exhibits a tripping point and has a large wall shear stress. The two transitional models, the original formulation and the pro-posed adjusted model, show a similar location for the tripping point. The transitional models show detachment and reattachment through oscillation in C_f . The adjusted model however maintains a lower wall shear stress after reattachment which results in a lower C_d prediction. Using a similar plot in figure 14, we see the effect of reattachment. The adjusted model shows the same tripping point for 4° but subsequent reattachment causes an increase in C_f . This explains the increased C_d prediction shown in 12 Looking at the simplest simulation of a smooth foil at 0°, we find the lift coefficient for all three models varied less than 3% but the newly proposed reduced order model had a 6% reduction in run time as compared to the original γ - $\tilde{Re}_{\theta t}$ model. The fully turbulent model completes in substantially shorter time, as it has 2 less equations to solve per iteration. While it seem that for less time a fully turbulent model provides a similar answer in terms of lift coefficient, the difference is evident in the boundary layer of the simulation. Figure 15 shows the change in k at 0.05 x/C along a line perpendicular to the surface.

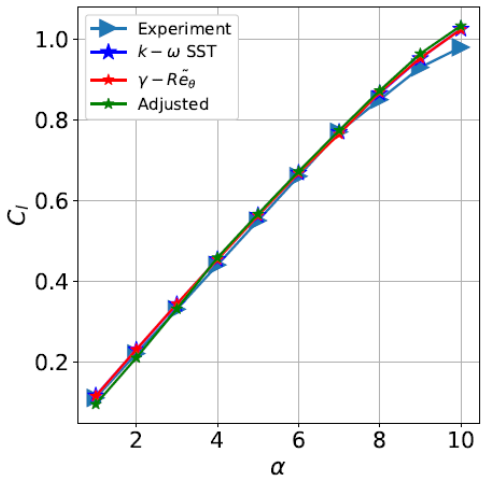

Fig. 11. C_l for NACA 0012 foil at Re 360 000.

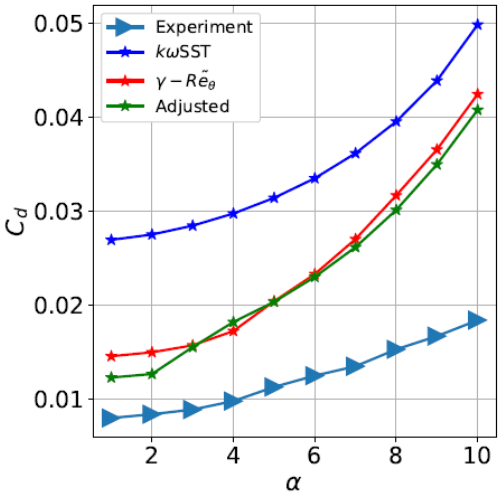

Fig. 12. C_d for NACA 0012 foil at Re 360 000.

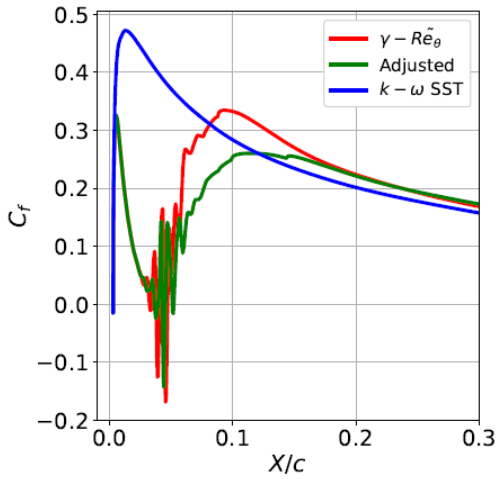

Fig. 13. C_f for NACA 0012 foil at Re 360 000, α=8.

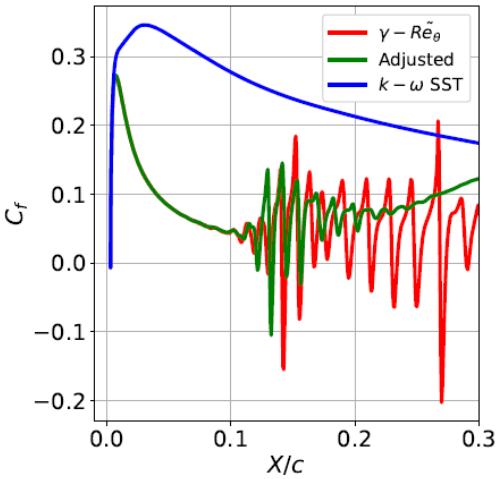

Fig. 14. C_f for NACA 0012 foil at Re 360 000, α=4.

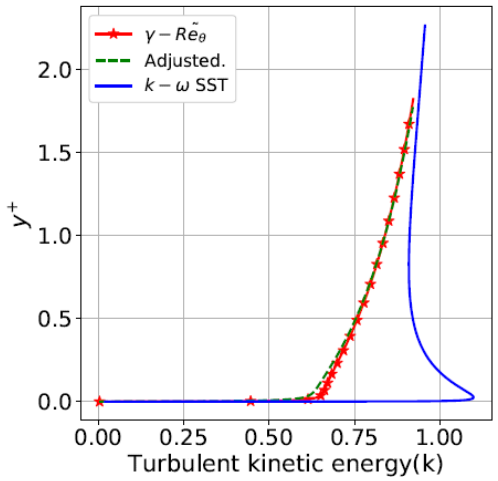

Fig. 15. Variation in k through the boundary layer.

On the foil surface there is zero turbulent kinetic energy and moving through the boundary layer k increases. The reduced order model is seen to compare well with the original formulation, in providing similar estimates for turbulent kinetic energy. The fully turbulent model shows a much larger k value closer to the wall, followed by a sudden drop. Turbulent kinetic energy is expected to increase as the distance from the wall increases due to the velocity increasing. The transitional models show this trend and converge within the boundary layer. All 3 models reach a similar value beyond a $y^+ \geq 2$.

Figure 16 shows the turbulent kinetic energy adjacent to a NACA 0012 with a distortion on the leading edge. The lower portion of the figure shows the leading edge upper surface of the foil.

The distortion was added to highlight the effect of the intermittency term for increasing k production. At 0.1 on the shared x-axis is the distortion. In the upper portion of the figure the resultant k for each turbulence model is plotted. Right before the flow encounters the distortion there is a large spike in k according to the fully turbulent model as compared to a smaller increase in the transition models. Post distortion the transition models have a bigger peak before settling to a lower nominal k than the turbulent model.

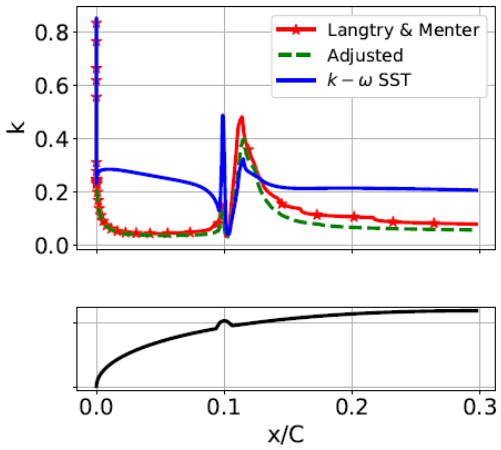

Fig. 16. Variation in k along foil length.

6. CONCLUSIONS

This work aimed to replace the complex empirically derived piecewise correlations used in the γ- $\tilde{R}e_{\theta t}$ turbulence model with more intuitive mathematical expressions. In identifying relationships between the empirical correlations it was important to take into account their interactions. The γ- $\tilde{R}e_{\theta t}$ model showed particular sensitivity to momentum thickness Reynolds number as a function of turbulence intensity (equation 5). Each correlation was replaced by simple mathematical expression, using a least squares best fit approach. Replacement of the individual equations (3 - 5) with suitable approximations did not result in an accurate model. Minor adjustments were made to the new equations resulting in an accurate prediction of skin friction on the T3A flat plate test case. Once validated the

adjusted model was tested on a NACA 0012 airfoil. The lift and drag values over a range of angles of attack were compared with experimental data. The adjusted model showed negligible difference when compared to the original γ -$\tilde{R}e_{\theta t}$ model for coefficients of lift. However a comparison of drag coefficients showed an improvement in prediction. Looking at the growth of turbulent kinetic energy through the boundary layer, the adjusted model very closely matched the original model. Further validating the adjusted model and proving its generality. Finally a comparison of behaviour between a fully turbulent and the adjusted model showed the benefits of using a transitional model, through a more realistic development of turbulent kinetic energy after the introduction of a distortion on the surface of an airfoil. The mathematical expressions proposed allowed for selection of the most influential coefficients and a more focused approach to adjusting the model. In addition it was shown that the proposed model reduced run time of simulations with no discernible decrease in accuracy. The expressions chosen for the correlations enable a user to more easily comprehend the effect of adjustments to their coefficients.

7. FUTURE WORK

As demonstrated the new model can be tailored to fit experimental data and it is proposed that this approach be used to improve the accuracy of the model for more complex geometries. The manual process used to adjust the coefficients was only suitable for a small simulation with a quick solution time. Larger, more complex simulations could also have the transition model adjusted but it is suggested that a surrogate model approach be utilised. A few simulations could be run to develop a work space that an optimisation algorithm could then explore, in order to reduce the error between experiments and CFD predictions.

ACKNOWLEDGEMENTS

This work would not be possible without the high performance computing facilities offered by the CSIR, in particular thanks to the CHPC-Rosebank for making their cluster available for testing.

REFERENCES

Langtry, R. and F. Menter (2005). Transition modeling for general CFD aapplication in aeronaurics. In *43rd AIAA Aerospace Sciences Meeting and Exhibit*.

Langtry, R. B. and F. R. Menter (2009, December). Correlation-based transition mod-model for unstructred parallelized computational fluid dynamics codes. *AIAA Journal* 47(12), 2894–2906.

Lanzafame, R., S. Mauro and M. Messina (2014). 2d cfd modeling of hdarrieus wind turbines using a transition turbulence model. *Energy Procedia* 45, 131–140.

Misaka, T. and S. Obayashi (2006). Application of local correlation-based transition model to flows around wings. In *44th AIAA Aerodspace Sciences Meeting and Exhibit*.

Savill, A. (1990). *Synthesis of t3 test case computations*. Proc. 1st. ERCOFTAC Workshop, Cambridge U. Press.

Savill, A. (1993). Some recent progress in the turbulence modelling of by-pass transition. Near-wall turbulent flows 829–848.

Savill, A. (1996). One-point closures applied to transition. In *Turbulence and transition modelling*, 233–268. Springer.

Sheldahl, R. E. and P. C. Klimas (1981). Aerodynamic characteristics of seven symmetrical airfoil sections through 180-degree angle of attack for use in aerodynamic analysis of vertical axis wind turbines. *Technical report, Sandia National Labs*., Albuquerque, NM (USA).

Sorensen, N. N. (2009). CFD modemodel of laminar-turbulent transition for airfoils and rotors using the γ - re model. *Wind energy* 12(8), 715–733.

Toyoda, A., T. Misaka and S. Obayashi (2007). Anapplicmodel of local correlation-based transition mode to jaxa high lift configuration model. In *25th AIAA Applied Aerodynamics Conference.*

Vanderspuy, S. J. (2011). *Perimeter fan performance in forced draught air-cooled steam condensers*. Ph. D. thesis, Stellenbosch: Stellenbosch University.

Vicedo, J., S. Vilmin, W. Dawes and A. Savill (2004). Intermittency transport modeling of separated flow transition. *Journal of turbo-machinery* 126(3), 424–431.

Weller, H. G., G. Tabor, H. Jasak and C. Fureby (1998). A tensorial approach to computational continuum mechanics using object-oriented techniques. *Computers in physics* 12(6), 620–631.